ADVANCED MATERIALS
www.advmat.de

Biomimetic Nanosilica–Collagen Scaffolds for In Situ Bone Regeneration: Toward a Cell-Free, One-Step Surgery

Shao-Jie Wang, Dong Jiang, Zheng-Zheng Zhang, You-Rong Chen, Zheng-Dong Yang, Ji-Ying Zhang, Jinjun Shi, Xing Wang,* and Jia-Kuo Yu**

Current approaches to fabrication of nSC composites for bone tissue engineering (BTE) have limited capacity to achieve uniform surface functionalization while replicating the complex architecture and bioactivity of native bone, compromising application of these nanocomposites for in situ bone regeneration. A robust biosilicification strategy is reported to impart a uniform and stable osteoinductive surface to porous collagen scaffolds. The resultant nSC composites possess a native-bone-like porous structure and a nanosilica coating. The osteoinductivity of the nSC scaffolds is strongly dependent on the surface roughness and silicon content in the silica coating. Notably, without the use of exogenous cells and growth factors (GFs), the nSC scaffolds induce successful repair of a critical-sized calvarium defect in a rabbit model. It is revealed that topographic and chemical cues presented by nSC scaffolds could synergistically activate multiple signaling pathways related to mesenchymal stem cell recruitment and bone regeneration. Thus, this facile surface biosilicification approach could be valuable by enabling production of BTE scaffolds with large sizes, complex porous structures, and varied osteoinductivity. The nanosilica-functionalized scaffolds can be implanted via a cell/GF-free, one-step surgery for in situ bone regeneration, thus demonstrating high potential for clinical translation in treatment of massive bone defects.

Reconstruction of massive bone defects has historically been an enormous challenge for both patients and orthopedic surgeons. Suitable materials for bone defect repair primarily include autografts, allografts, and artificial bone scaffolds for tissue regeneration.[1–4] Although autografts are the gold standard in clinical practice, they pose significant potential complications, including limited bone mass, size mismatch, low availability, and donor site damage. Allogenic bone grafts also frequently lead to potential risks, such as disease transmission, contamination, and immunological rejection if donors are not adequately evaluated or serologically screened. Fortunately, advancements such as lab-constructed bone tissue engineering (BTE) scaffolds containing in vitro expanded cells have provided promising biomimetic bone options for patients. However, this approach involves extensive ex vivo cell manipulation, potential tumorigenesis, and difficulties in therapeutic translation and regulatory approval.[5a] To circumvent these problems, utilization of the recipient's endogenous cells for in situ tissue regeneration is a practical strategy that eliminates the need for exogenous cells. This viable BTE strategy requires the bioscaffolds to effectively recruit host stem or progenitor cells to the injury site while providing a proper niche for the recruited cells to differentiate into bone-specific cell lineages.[5b]

Dr. S.-J. Wang, Dr. D. Jiang, Dr. Z.-Z. Zhang, Dr. Y.-R. Chen, J.-Y. Zhang, Prof. J.-K. Yu
Knee Surgery Department of the Institute of Sports Medicine
Beijing Key Laboratory of Sports Injuries
Peking University Third Hospital
Beijing 100191, China
E-mail: yujiakuo@126.com
Dr. S.-J. Wang
Department of Joint Surgery and Sports Medicine
Zhongshan Hospital
Xiamen University
Xiamen, Fujian 361000, China
Dr. Z.-Z. Zhang
Department of Orthopedics
Sun Yat-sen Memorial Hospital
Sun Yat-sen University
Guangzhou 510120, China
The ORCID identification number(s) for the author(s) of this article can be found under https://doi.org/10.1002/adma.201904341.
Z.-D. Yang
Department of Chemistry
University of California Riverside
Riverside, CA 92521, USA
Prof. J. Shi
Center for Nanomedicine
Brigham and Women's Hospital
Harvard Medical School
Boston, MA 02115, USA
E-mail: jshi@bwh.harvard.edu
Dr. X. Wang
Beijing National Laboratory for Molecular Sciences
State Key Laboratory of Polymer Physics and Chemistry
Institute of Chemistry Chinese Academy of Sciences
Beijing 100190, China
E-mail: wangxing@iccas.ac.cn

DOI: 10.1002/adma.201904341

Incorporation and administration of various growth factors (GFs) into these bioscaffolds have been commonly used to improve mesenchymal stem cell (MSC) recruitment and bone healing, but concerns still exist regarding the risks of GF use, such as their short half-life, high price, rapid degradation, immunogenicity, and possible toxicity and tumorigenicity.[6] Consequently, it is particularly challenging and significant to develop an ideal cell- and GF-free scaffold that can recruit host cells and promote osteogenesis upon implantation.

Nanocomposite biomaterials can mimic the unique microenvironmental signals present in the bone extracellular matrix (ECM), providing various structural, mechanical, and biological cues to guide survival, proliferation, and proper differentiation of MSCs. Bone ECM can serve as a unique nanocomposite consisting of natural collagen (mainly collagen type I, COL1) fibers and inorganics. Osteoinductive materials with native bone ECM components have been orchestrated to create collagen/inorganic composites. These synthetic bone grafts have attracted significant attention due to their ability to mimic the biochemical composition, biophysical structure, and mechanical properties of native bone ECM.[7] Silicon (Si) is an essential trace element required for metabolic processes associated with connective tissue development and bone metabolism.[8] The significant roles Si ions have in triggering osteogenic differentiation of MSCs include promoting bone matrix deposition and mineralization and recruiting MSCs. To avoid the issues associated with the resorbability and brittleness of hydroxyapatite-collagen scaffolds, silica has become a potential alternative or supplement to hydroxyapatite due to its similar osteoinduction capacity.[8c] Current strategies for silicification of collagen scaffolds, such as bulk silica modification and intrafibrillar silicification, have been well-developed to fabricate osteogenesis-enhancing silica-collagen composites.[1,9a,b] These strategies often utilize a polyamine to catalyze silica polymerization and control the morphology and structure of silica oxide complexes.[9c,d] However, to form a continuous and stable silica layer, a high density of organic compounds must be deposited on the surface of the material (the higher the degree of surface modification, the greater the silica coverage).[9e,f] In addition, most Si-containing inorganics are encapsulated by the collagen matrix of silica-collagen composites, severely limiting adequate release of the Si ions and their direct interaction with surrounding cells. More importantly, these silica-collagen composites cannot precisely recapitulate the natural bone with respect to the intricate surface topographies and hierarchical porous architectures that are critical to sustain cell–material biophysical interactions.[10]

Herein, we developed a robust functionalization strategy through a facile surface silicification process to fabricate porous nanosilica-collagen (nSC) scaffolds derived from porcine demineralized cancellous bone (DCB) to promote bone regeneration without the need for cells or GFs (**Figure 1**). The nanosilica-modified collagen possesses inherent hierarchical pores with a sturdy nanoroughened surface, an organic-collagen/inorganic-silica composition, and enhanced mechanical properties. As verified by in vitro and in vivo experimental results, the biophysical and biochemical cues presented by nSC scaffolds provide a structurally and chemically biomimetic microenvironment that promotes host MSC recruitment, proliferation, and osteogenesis for superior bone defect repair. The benefits of this strategy are as follows: (1) The facile surface biosilicification generates uniform and complete internal and external surface coverage of a nanosilica coating throughout the complex porous structure of the collagen scaffold; (2) The topographically and chemically biomimetic surface endows nSC composites with high osteoinductivity to promote host MSC recruitment and proliferation, osteogenesis, and matrix mineralization; (3) One-step surgical implantation can effectively repair large defects in rabbit calvarium through endogenous bone regeneration without the use of exogenous MSCs or GFs. We believe that this robust, effective, and simple biosilicification strategy could be universally applicable in development of BTE scaffolds with a large size and complex structure for enhanced in situ bone regeneration, and these scaffolds have great clinical translation potential for treatment of massive bone defects.

Although porcine DCB possesses open and interconnected pores beneficial for BTE applications, its osteoinductivity is limited by a smooth collagen surface and by depletion of inorganic substances and osteogenic proteins secondary to the demineralization and deproteinization processes that remove immunogenic material. Therefore, we used a prefabricated collagen scaffold derived from porcine DCB as a template for in situ surface biosilicification using three types of silica precursors: (3-aminopropyl)trimethoxysilane (APTMS), (3-mercaptopropyl)trimethoxysilane (MPTMS), and tetramethoxysilane (TMS), and the resultant scaffolds were referred to as AP-nSC, MP-nSC, and T-nSC, respectively.

To prepare a uniform and sturdy functionalized surface with enhanced osteoconductivity, it is necessary to form a continuous and stable silica coating to control the topographic features and the amount of silica coating (the higher the surface modification density, the better the silicon coating coverage). Therefore, we adopted a straightforward LBL method. Three bilayers of PDADMAC/PAA-g-AB were first adsorbed to the surface of a DCB scaffold, and then, DMAEMA was polymerized onto the surface via ATRP. Subsequently, silica polymerization was induced to produce positively charged amino groups under relatively mild conditions (Figure 1). The pure DCB scaffold (negative control) exhibited a highly open, interconnected porous structure, with an average pore size of 344.2 ± 83.8 μm and a porosity of 88.8 ± 4.5%. These specific hierarchical pores of DCB-derived scaffolds are critical for cell infiltration, osteogenesis, and tissue in-growth. Larger pore sizes (>300 μm) in nSC composites are beneficial for new bone and capillary regeneration, while smaller pores have been shown to result in hypoxic conditions that induce chondrogenesis.[11] AP-nSC, MP-nSC, and T-nSC scaffolds exhibited similar pore morphology, pore size (399.9 ± 78.2, 347.6 ± 72.5, and 385.6 ± 91.6 μm, respectively), and porosity (89.1 ± 4.5, 85.6 ± 4.0, and 88.4 ± 5.2%, respectively) (Figures S1 and S2, Supporting Information), suggesting that the biosilicification process produced minimal disruption to the porous architecture and therefore the nSC composites preserved the natural bone-like porous architecture of the untreated DCB collagen scaffold.

The surface topography and roughness of collagen scaffolds are critical to replicating the complex architecture of natural bone.[12] Upon nanosilica functionalization, the collagen scaffold surfaces exhibited rougher topography relative to control DCB, verified by scanning electron microscopy (SEM) and atomic

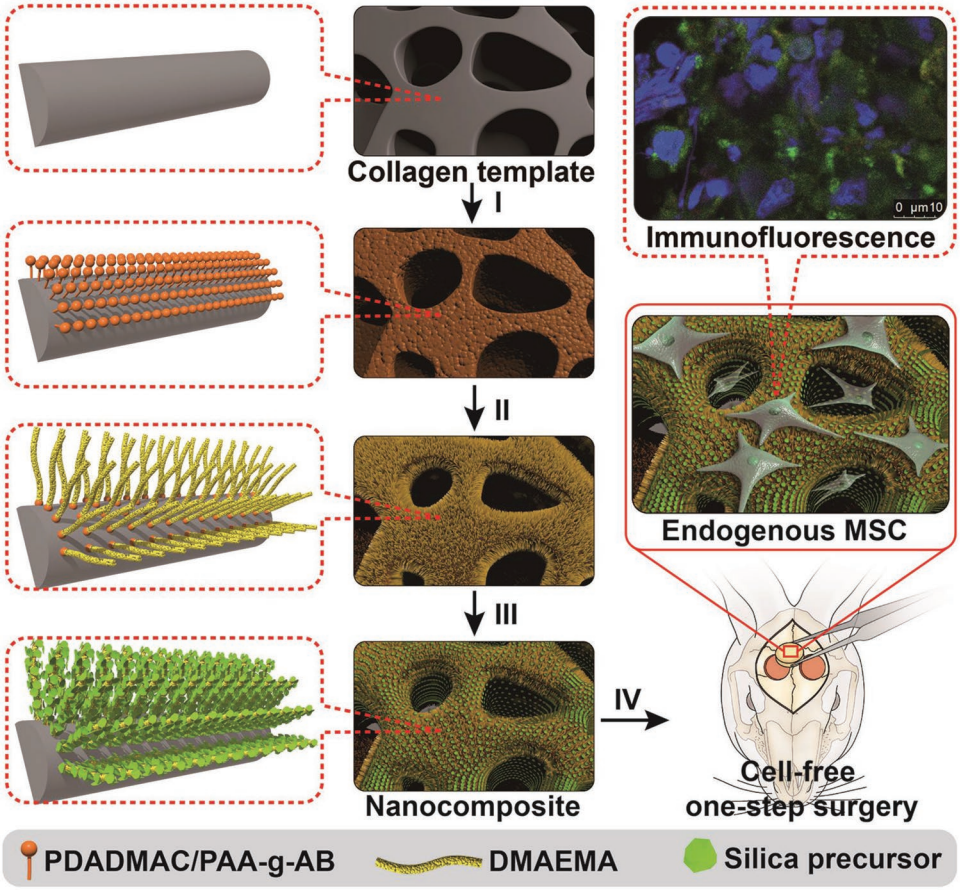

Figure 1. Scheme of nanosilica modification process on the surface of collagen scaffolds and the cell-free, one-step implantation approach for bone defect repair. (I) Layer-by-layer (LBL) adsorption of poly(diallyldimethylammonium chloride) (PDADMAC)/poly(acrylic acid-*g*-alkyl bromide) (PAA-*g*-AB) on the porous collagen scaffold as a template; (II) 2-(dimethylamino)ethyl methacrylate (DMAEMA) is polymerized via atom transfer radical polymerization (ATRP); (III) polymerization of silica precursors is initiated to obtain homogeneously modified nSC scaffolds; (IV) implantation of the cell-free functionalized collagen scaffold enhances bone regeneration by improving host MSC recruitment and osteogenesis.

force microscopy (AFM) imaging ($n = 5$, $p < 0.05$) (**Figure 2**A,B). X-ray photoelectron spectroscopy (XPS) confirmed surface silicification by showing the presence of Si peaks with varying intensities in the nSC composites and the expected absence of these peaks in the DCB scaffold (Figure 2C; Figure S3 and Table S1, Supporting Information). Among the nSC scaffolds, T-nSC had the richest deposition of silica, which can be explained by the negative charge of silanol groups induced through hydrolysis of TMS, which may facilitate interaction with the superficial PDMAEMA that contains positively charged tertiary amines.[13] In contrast, the positive charge of the amino groups in APTMS is believed to have severely hindered silica deposition onto the PDMAEMA template due to charge repulsion, leading to reduced silica deposition onto the AP-nSC scaffold surfaces. Semiquantitative analysis results showed that the surface roughness of the scaffolds decreased in the following order: T-nSC > MP-nSC > AP-nSC > DCB, which is consistent with the extent of silicon deposition (Figure 2D). Notably, in contrast with traditional surface modification methods (e.g., plasma treatments), this biosilicification approach resulted in omnidirectional nanosilica coating throughout the entire scaffold surface. Energy-dispersive X-ray spectroscopy (EDS) elemental mapping demonstrated that cross-sectional surfaces of the scaffolds contained amounts of Si similar to those found on the exterior surface of the scaffolds (Figure S4, Supporting Information). These findings demonstrate that this facile biosilicification process yielded excellent and uniform distribution of silica throughout the porous scaffolds. The complete surface coverage of the silica coating is particularly important in fabricating osteoinductive scaffolds with a large size and complex structures for application in large bone defect repair.

The nanosilica coating significantly enhanced the mechanical properties of the nSC composites (**Figure 3**A,B; Figure S5, Supporting Information). The hardness and reduced modulus of DCB (7.0 ± 3.2 MPa and 0.3 ± 0.1 GPa, respectively) increased significantly with addition of the silica coating ($n = 5$, $p < 0.05$). The highest hardness and reduced modulus values were found for the T-nSC scaffold (32.9 ± 0.1 MPa and 1.0 ± 0.2 GPa, respectively). Scaffold sturdiness (i.e., high hardness and reduced modulus) can prevent early collapse, enabling sustainable release of Si ions and facilitating accessibility of cell substrates, which are necessary for nSC scaffolds to be effective in BTE applications in mechanically challenging physiological environments. As expected, the DCB, AP-nSC, MP-nSC, and

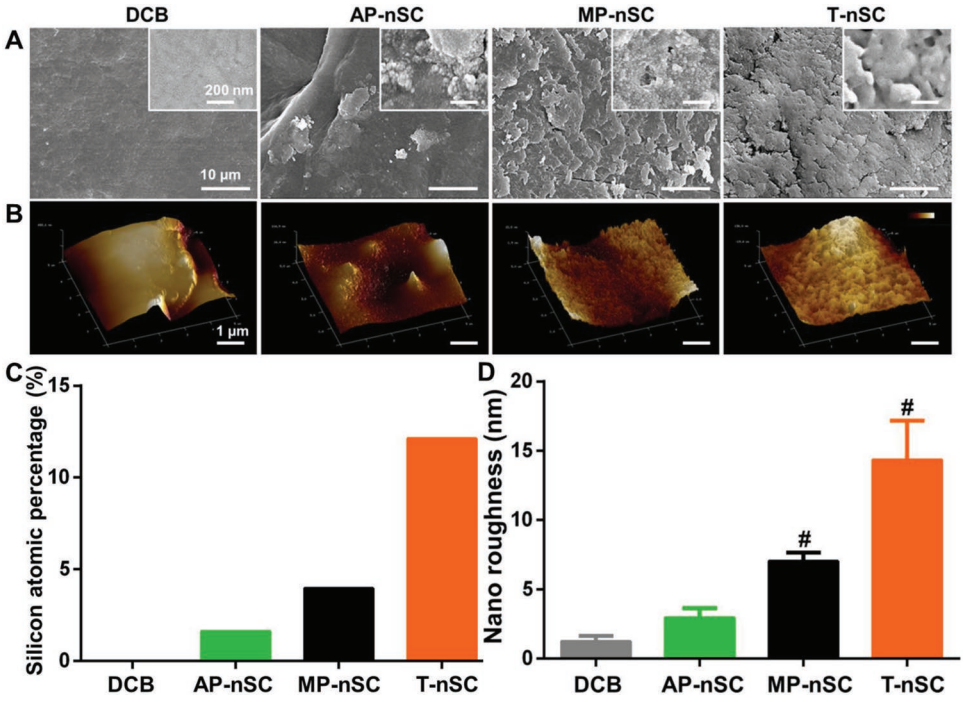

Figure 2. A) FESEM and B) AFM images showing the surface topologies of DCB, AP-nSC, MP-nSC, and T-nSC scaffolds. C) XPS analysis of the silicon atomic percentage in the scaffolds. D) AFM analysis of the surface roughness of the scaffolds ($n = 5$). $^{\#}p < 0.05$ compared with DCB at matching time points.

T-nSC scaffolds exhibited various Si ion release kinetic behaviors (Figure 3C), with mean release concentrations of 2.73, 7.63, 16.04, and 24.61 μg mL^{-1}, respectively, at day 21 in culture medium, far below the toxic level (200 μg mL^{-1}).[14] Live/Dead staining of bone marrow MSCs (BMMSCs) seeded on scaffolds was performed after incubation for 3 d. As shown in Figure 3D, a high percentage of the BMMSCs were viable and adhered along the pore walls (Figure S6, Supporting Information), indicating the biocompatibility and biosafety of nanosilica-modified collagen scaffolds.

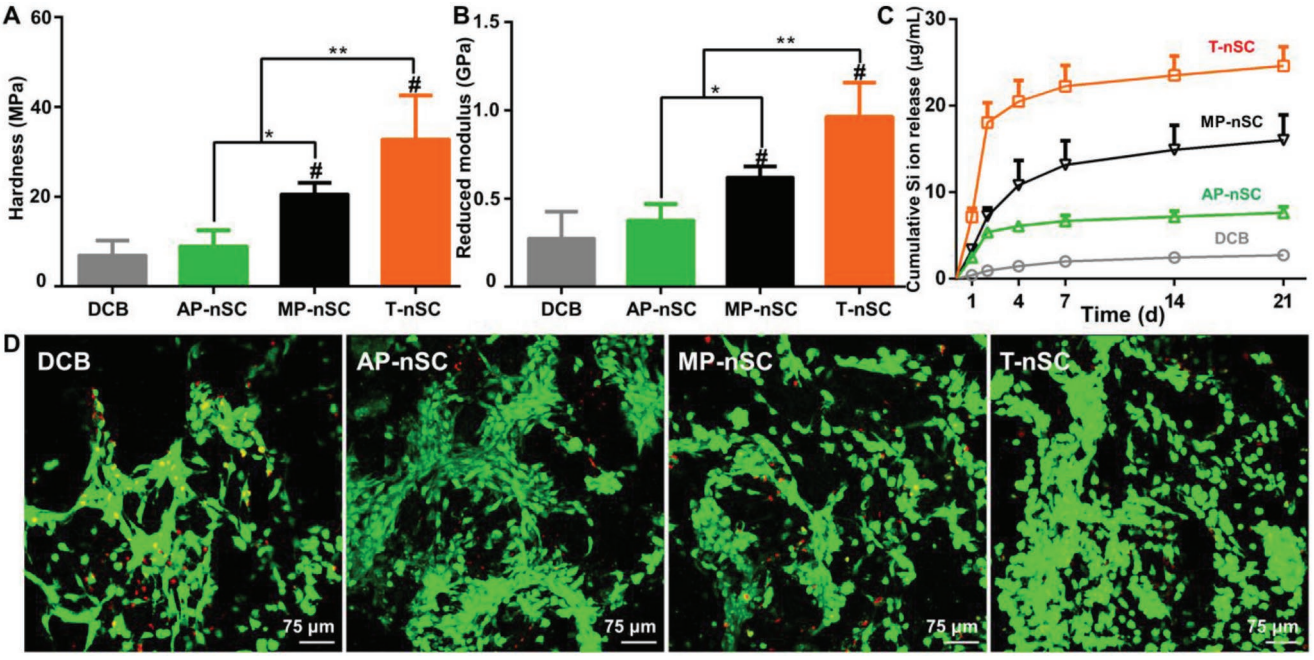

Figure 3. A) Hardness and B) reduced modulus of DCB and nSC scaffolds ($n = 5$, $^{*}p < 0.05$, $^{**}p < 0.01$; $^{\#}p < 0.05$ compared with DCB at matching time points). C) In vitro Si ion release profiles of DCB and nSC scaffolds. D) Live/Dead staining to assess viability of cells cultured on DCB and nSC scaffolds.

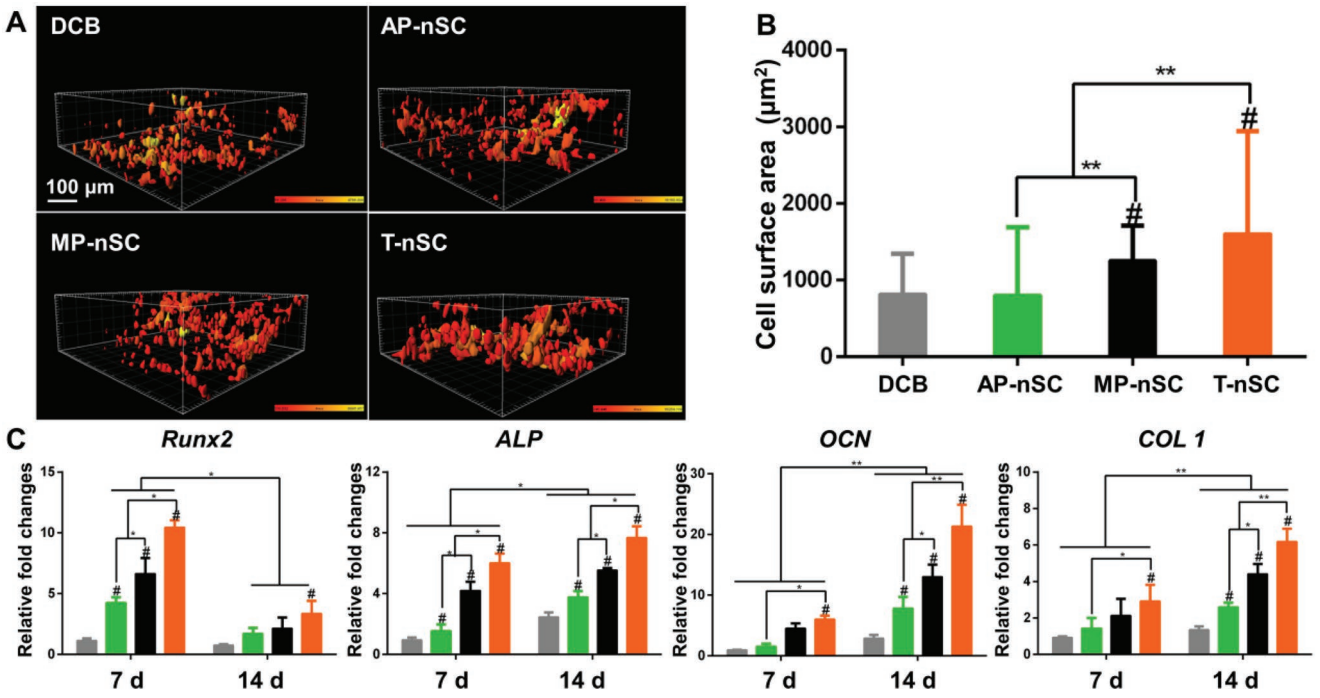

Figure 4. A) 3D rendering images and B) quantitative results showing cell surface areas in scaffolds with increasing silicon content and surface roughness (from DCB to T-nSC) (**$p < 0.01$; #$p < 0.05$ compared with DCB at matching time points). C) RT-PCR detection of in vitro expression of the bone-specific genes *Runx2*, *ALP*, *OCN*, and *COL1* at days 7 and 14 ($n = 3$, *$p < 0.05$, **$p < 0.01$; #$p < 0.05$ compared with DCB at matching time points).

The topographic and chemical cues presented by scaffold surfaces significantly affect cell–material interactions, such as adhesion, spreading, and differentiation.[15] After BMMSCs were cultured in osteogenic medium without dexamethasone for 21 d, BMMSC osteogenesis was verified by assessing the in vitro expression levels of bone-specific genes, including runt-related transcription factor (*Runx2*), alkaline phosphatase (*ALP*), osteocalcin (*OCN*), and collagen type I (*COL1*). To reveal the influence of the nanosilica coating on BMMSC spreading in the scaffolds, we used calcein AM to stain the cytoplasm and calculate the virtual surface area of the cells. With increasing Si content and surface features (T-nSC > MP-nSC > AP-nSC > DCB), the BMMSCs in the nSC composites displayed larger cell surface areas at day 7 (**Figure 4**A) and greater osteogenic gene expression levels at days 7 and 14 compared with those in DCB (Figure 4B,C; Table S2, Supporting Information). The cell spreading and osteogenic gene expression levels followed the same order as the silicon content and surface roughness, which strongly supports the notion that the nanosilica-modified collagen scaffolds effectively improve cell–material interactions and promote osteogenic differentiation of BMMSCs.

Single and double stimulus culture models were utilized to further distinguish the effects of Si ions and surface roughness of the nSC scaffolds on the proliferation and osteogenesis of BMMSCs. The single-stimulus culture method solely tested the response to Si ions and demonstrated a similar cell proliferation rate among the nSC composite and DCB groups. In contrast, the double-stimulus model, in which response to stimulus with both Si ions and roughened surfaces was assessed, showed significantly higher cell proliferation rates in all nSC composite groups than in the DCB groups after 7 d, with T-nSC fostering the highest cell proliferation rate (**Figure 5**A). Although high concentrations of Si ions in the single-stimulus culture obviously induced BMMSCs to produce high levels of ALP activity and osteogenic markers (OCN and COL1), the levels of these markers were further increased by the double-stimulus culture (Figure 5B), suggesting that the combined effects of Si ions and roughness on the proliferation rate and osteogenesis of BMMSCs were greater than that of Si ions alone. Notably, the T-nSC scaffold presented the highest ability to enhance BMMSC proliferation and osteogenesis, revealing the substantial influence of biosilicification of scaffold surfaces on enhanced cell proliferation and osteogenic differentiation.

Having achieved promising in vitro results regarding the osteoinductivity of nSC scaffolds for BMMSC osteogenesis, we further evaluated the effects of nSC scaffolds on in vivo bone matrix maturation by examining calcified matrix deposition in a subcutaneous implantation nude mouse model. Semiquantitative analysis of Alizarin Red staining revealed that T-nSC scaffolds supported the highest and most uniform calcium deposition, followed by MP-nSC scaffolds with intermittent calcium deposition, and AP-nSC scaffolds with sparse calcium deposition (87.5 ± 1.4, 39.4 ± 3.3, and 18.9 ± 0.9%, respectively) (**Figure 6**A,B). Calcium deposition was shown to be minimal on the noncoated DCB scaffold (2.1 ± 1.4%). The extent of matrix mineralization may be related to the contribution of the silica-functionalized surfaces to osteogenesis induction and collagen production, as well as the Si ion release, which has been found to effectively accelerate generation of mineralized nodules.[8] Additionally, an abundance of negatively charged silanol groups (Si—OH) of the nanosilica on nSC scaffolds may produce

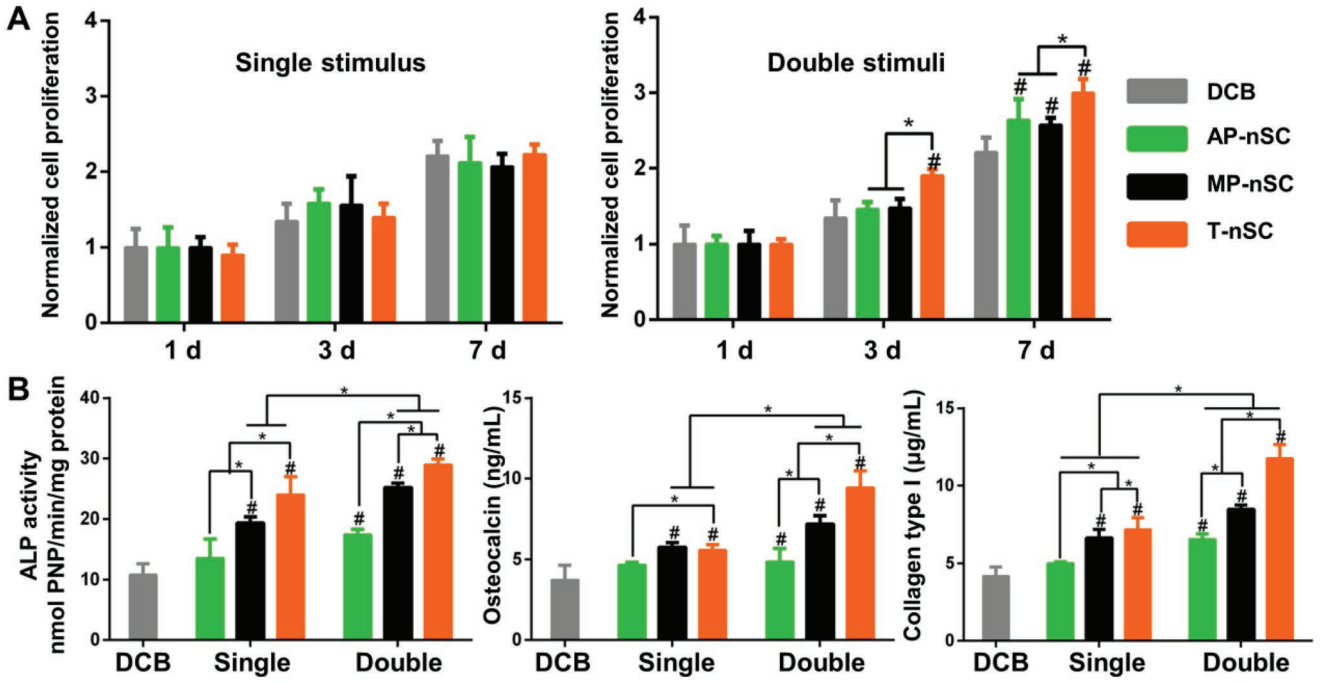

Figure 5. A) CCK-8 assay to assess BMMSC proliferation in single- or double-stimulus culture models ($n = 4$; $^{*}p < 0.05$; $^{\#}p < 0.05$ compared with DCB at matching time points). B) In vitro ALP activity and OCN and COL1 secretion in single- or double-stimulus culture models after 21 d of culture in osteogenic medium without dexamethasone ($n = 3$; $^{*}p < 0.05$; $^{\#}p < 0.05$ compared with DCB at matching time points).

strong interactions with mineral ions in the surrounding environment, thus leading to increased matrix calcification.[16]

To further evaluate the nSC scaffold capacity to recruit host MSCs for endogenous bone regeneration, cell-free scaffolds were implanted into calvarium defects in rabbits. One week after surgery, the implanted scaffolds were retrieved and subjected to immunofluorescence staining to locate cells positive for the mesenchymal marker CD29 and negative for the hematopoietic marker CD45. Frozen sections and immunofluorescence staining illustrated that host cells with an MSC phenotype ($CD29^{+}$ $CD45^{-}$) were present in all nSC scaffolds and that the number of recruited MSCs, particularly in the T-nSC scaffold group, exceeded that in the DCB group ($n = 3$, $^{*}p < 0.01$) (Figure S7, Supporting Information). These results suggest a direct correlation between the extent of functionalization and Si ion release and MSC recruitment, which might induce subsequent osteogenesis of MSCs and neo-bone formation. Furthermore, we implanted MSC-free scaffolds into calvarial defects with a critical size of 8 mm in a rabbit model to investigate the recruited MSC differentiation and subsequent regeneration of functional bone tissue. As expected, micro-CT analysis and the HE and MT staining results showed expedited and more extensive endogenous bone regeneration in the nSC scaffold groups compared with the DCB control groups at weeks 6 and 12 after implantation (Figure 6C,D; Figure S8, Supporting Information). PR staining clearly indicated maturity of the regenerated bone tissue (Figure 6D). Specifically, the T-nSC scaffolds generated more mature bone exhibiting parallel collagen fibers (stained yellow-green) than MP-nSC and AP-nSC scaffolds, which yielded immature bone-like tissues with less ordered collagen fibers (stained red and partially green). In contrast, disorganized fibrous tissue infiltrated the DCB scaffold (stained red). These results are also supported by the literature in regard to the active involvement of Si ions in matrix synthesis, maturation, and turnover to maintain matrix stabilization.[17] Therefore, these nSC composites indeed provide a natural bone ECM-mimicking niche for endogenous cells to attach, grow, and differentiate into mature bone tissue and thus present a superior capacity for enhanced bone regeneration.

To explore the potential molecular mechanisms underlying enhancement of bone formation resulting from host MSC interactions with the nSC scaffold surface, we performed RNA sequencing (RNA-seq) to compare gene expression profiles of MSCs cultured with DCB and nSC scaffolds. PCA revealed that differential gene expression was considerably correlated with the type of scaffold used (**Figure 7**A); in other words, the type of scaffolds could determine the gene expression profile of MSCs (Table S3, Supporting Information). Among the differentially expressed (DE) genes, only those demonstrating an ascending or descending gene expression trend were selected for further analysis. As shown by the gene profiling results presented as a heatmap in Figure 7B, 450 genes were significantly upregulated ($P < 0.05$) in an ascending order of AP-nSC and DCB < MP-nSC < T-nSC, while 72 genes were significantly downregulated ($P < 0.05$) in a descending order of T-nSC < MP-nSC < AP-nSC and DCB. Notably, T-nSC scaffolds exhibited the most substantial differential gene expression compared with the other nSC scaffolds. GO and KEGG enrichment analyses were performed to reveal the biological functions of these DE genes. GO analysis demonstrated that the upregulated and downregulated genes were involved in biological adhesion, binding, signaling, cellular processes, biological regulation, and cell

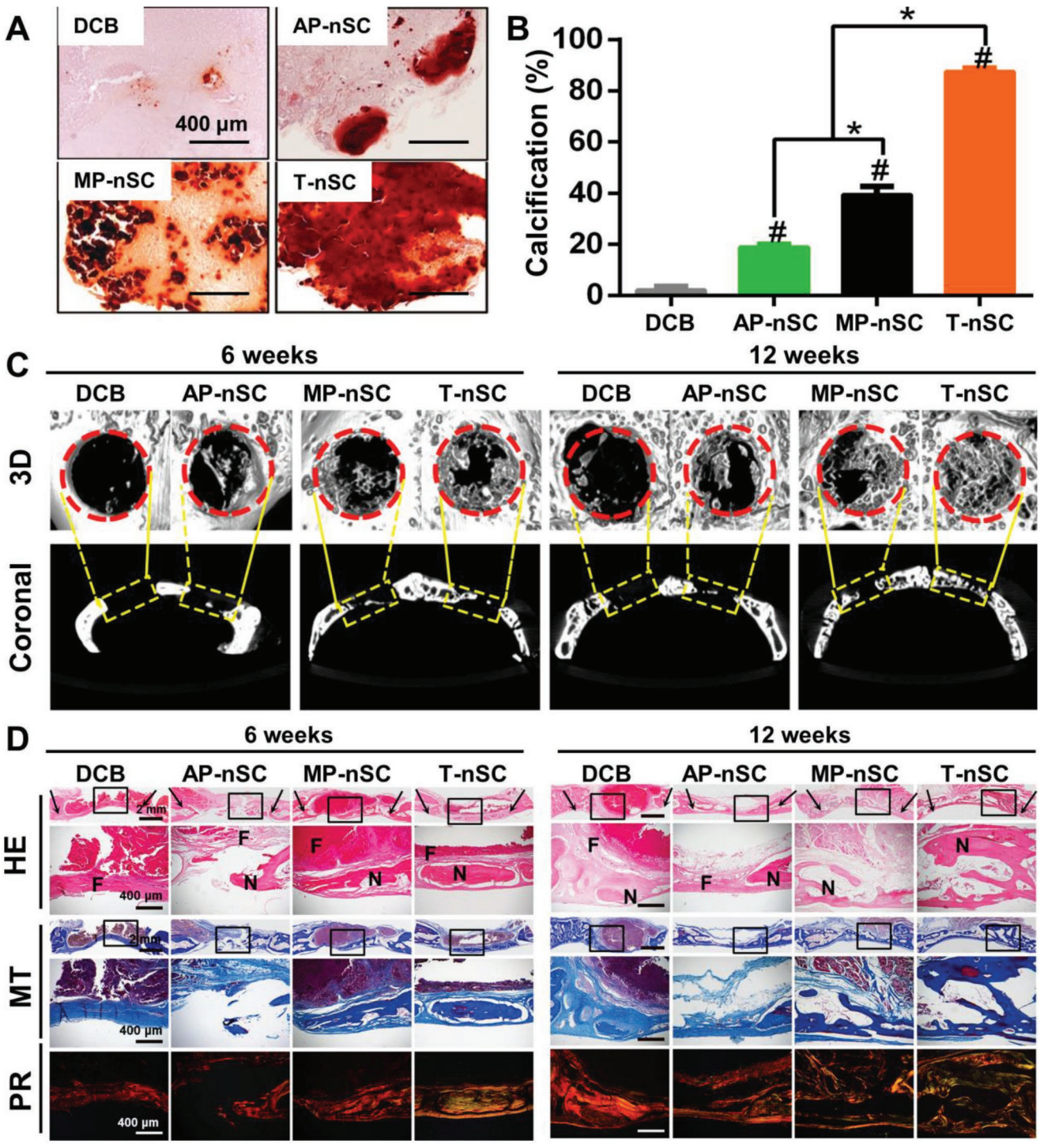

Figure 6. A) Alizarin Red staining images showing calcium deposition onto subcutaneous BMMSC-seeded scaffolds. B) Calcification of BMMSC-seeded scaffolds in nude mice at three weeks ($n = 6$; $^{*}p < 0.05$, $^{\#}p < 0.05$ compared with DCB at matching time points). C) Representative 3D images of coronal sections of a calvarium defect in a rabbit model at 6 and 12 weeks after implantation of scaffolds without exogenous MSCs. Red circles and yellow boxes define the defect margins. D) Hematoxylin and eosin (HE), Masson's Trichrome (MT), and Picrosirius Red (PR) staining demonstrating the formation of new bone after implantation of scaffolds in calvarium defects. Black arrows define the boundary of the defects. Lower panels present high-power views of the black rectangles in the upper panels (N: new bone; F: fibrous tissue; MT blue: new bone; MT bright red: mature bone; MT dark red: fibrous tissue).

junction formation (Figure S9, Supporting Information). KEGG pathway analysis of the upregulated genes revealed a significant enrichment of signaling pathways related to cell adhesion, proliferation, and differentiation into osteoblasts (Figure S10,

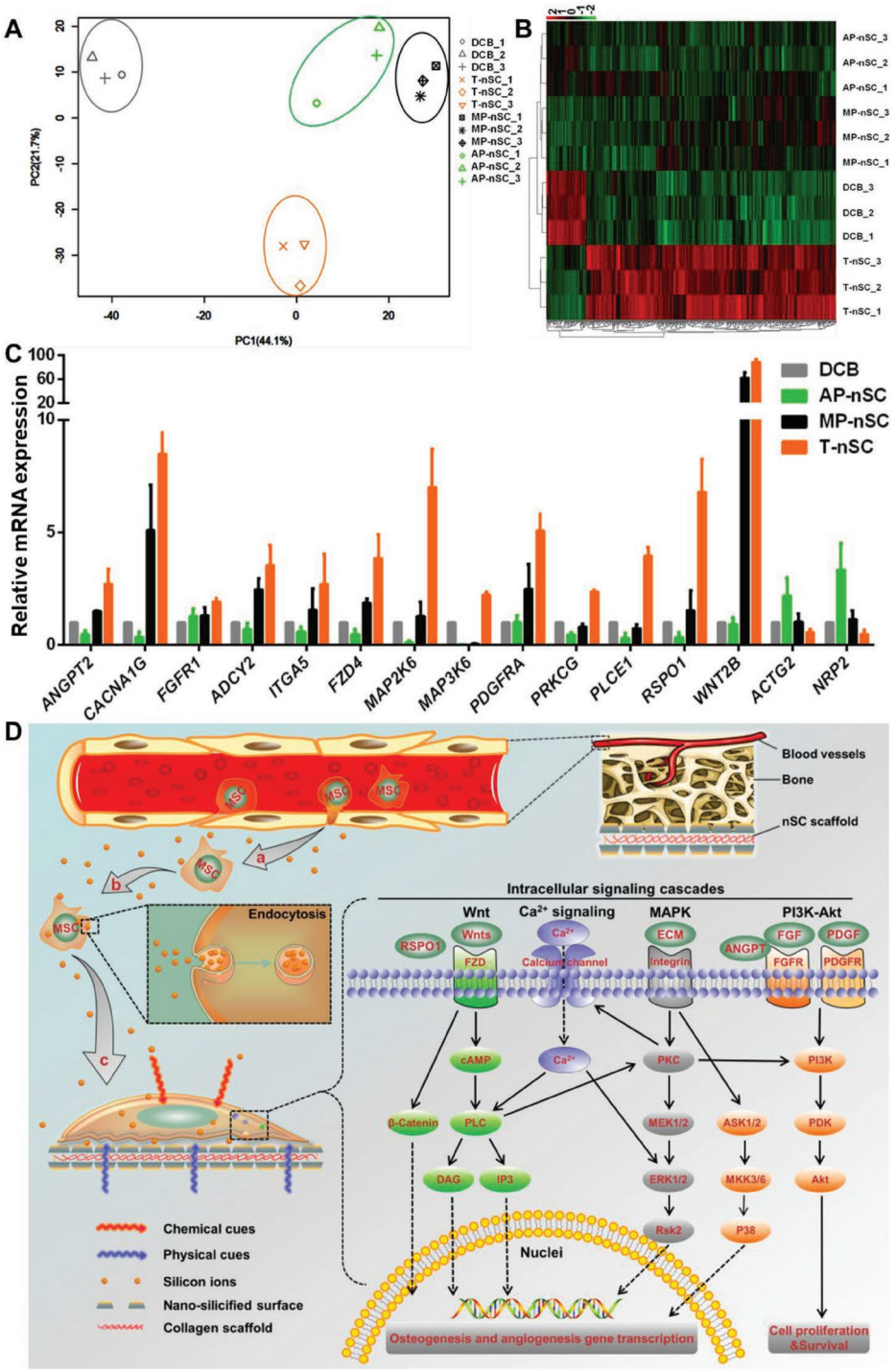

Figure 7. A) Variations in the RNA-seq data conveyed by principal component analysis (PCA) showing a correlation between groups of scaffolds (circles) and gene expression profiles. The distance between groups is proportional to the difference between gene expression profiles. B) Heatmap and hierarchical clustering analysis of differentially expressed genes among various scaffold groups. Each row represents the expression profile of a tissue sample, and each column corresponds to mRNA with a log fold change ≥2 ($P < 0.05$). Red indicates upregulated mRNA, while green represents downregulated mRNA. C) Quantitative real-time PCR (RT-PCR) analysis of the RNA-Seq. The data are presented as the mean ± SD of the three experiments. D) Scheme showing the proposed molecular mechanism of host MSC recruitment induced by chemical and physical cues presented by the nanosilica-functionalized composite surfaces to promote MSC differentiation and new bone formation. (a) MSCs and monocytes take up Si ions via endocytosis, and host MSCs are further recruited by the chemoattractants SDF-1 and TGF-β, secreted by monocytes; (b) MSCs express platelet-derived growth factor receptor (PDGFR), the receptor for the chemoattractant PDGF; (c) MSCs adhere to the nSC scaffold, triggering a series of intracellular osteogenesis-related signaling pathways, including the Ca^{2+} signaling, Wnt, MAPK, and PI3K-Akt pathways, due to the silica functionalization and surface features. Abbreviations are listed in the Appendix in the Supporting Information.

Supporting Information). These pathways included ECM-receptor interactions (ocu04512), MAPK signaling pathway (ocu04010), calcium signaling pathway (ocu04020), PI3K-Akt signaling pathway (ocu04151), and focal adhesions (ocu04510). On the other hand, the downregulated genes were enriched in cGMP-PKG signaling pathways, which regulate vascular smooth muscle contraction (ocu04270) (Figure S10, Supporting Information). From the above signaling pathways, 15 genes were selected for RT-PCR validation. As expected, the results for 13 upregulated genes (*PLCE1, PDGFRA, FGFR1, MAP2K6, MAP3K6, ANGPT-2, ITGA5, WNT2B, RSPO1, CACNA1G, FZD4, ADCY2, PRKCG*) and two downregulated genes (*NPR2, ACTG2*) were consistent with the above RNA-seq data (Figure 7C and Table S4, Supporting Information).

Based on the above data, it was speculated that host MSCs could be recruited to the nSC scaffolds in response to the release of Si ions (Figure 7D) because recent evidence suggests that silicic acid released from scaffolds can effectively recruit endogenous MSCs by promoting the release of MSC chemoattractants, such as stromal cell-derived factor-1 (SDF-1) and transforming growth factor-β1 (TGF-β1), from blood-derived monocytes.[9b] Moreover, the upregulation of PDGFR suggested that the Si ions from the nSC surface could enhance PDGFR expression on MSCs. Specifically, PDGFRs have an influential role in MAPK and PI3K signaling pathways that direct cell migration and proliferation.[18] Furthermore, the nSC scaffold topography and surface chemistry are believed to regulate multiple cellular signaling pathways to form a fine network that potentiates MSC recruitment, adhesion, proliferation, and osteogenesis, as well as vascularization and matrix mineralization (Figure 7D). The increased integrin binding and focal adhesion formation (*ANGPT2, FGFR1, ITGA5, PDGFRA*) can lead to activation of a series of signaling pathways, including PI3K-Akt (*ANGPT2, FGFR1, PDGFRA*) and MAPK (*PRKCG, MAP2K6, MAP3K6*) pathways.[19] With the help of PKC, Ca^{2+} influx into cytoplasm via calcium channels could activate the phospholipase C (*PLCE1*) and WNT/Ca^{2+} signaling pathways (*WNT2B, CACNA1G, ADCY2, CACNA1G, FZD4, RSPO1*).[20a] The cGMP-PKG signaling pathway (*NPR2*) downregulation may be the result of increased cytoplasmic Ca^{2+} concentrations that enhance the activity of cGMP-specific phosphodiesterase, which consequently decreases the amount of cGMP and activated MEK.[20b] For concurrent endochondral ossification with MSC osteogenesis, vascularization of the bone matrix is critical.[20c] Angiopoietin-2 (encoded by *ANGPT2*), which was shown to be upregulated in this study, is an established protein involved in angiogenesis and thus may play a role in driving the vascularization process in the bone matrix during osteogenesis.[20d] Therefore, the decrease in vascular smooth muscle contraction pathway proteins (*NPR2, ACTG2*) may be explained by an increase in blood flow to the bone defect area to promote bone healing.[18] This process has also been found to participate in endochondral ossification during skeletal tissue development.[20b]

In summary, we report a facile and feasible surface biosilicification method to construct nanosilica-modified collagen scaffolds that achieved effective in situ bone regeneration in large defects in rabbit calvarium without use of exogenous MSCs or GFs. Careful fabrication of various silica precursors on the porous DCB collagen template could tailor the osteoinductivity of nSC scaffolds, leading to high potency. The biosilicification process furnished these nSC scaffolds with topographical and chemical cues to create an osteoinductive extracellular milieu that promoted host MSC recruitment and osteogenesis and neo-tissue mineralization. Notably, in vivo studies confirmed that the nSC scaffold with the highest nanosilica functionalization, T-nSC, achieved excellent repair of a large calvarium defect without the use of exogenous MSCs or GFs. Concentrated release of Si ions and surface topography were shown to synergistically activate a series of signaling pathways associated with osteogenesis and vascularization. With these collective findings, this intriguing work provides an innovative and universal approach to improve the osteoinductivity of scaffolds with large sizes and complex structures. The excellent osteoinductivity of the nanosilica-functionalized scaffolds allows for in situ bone regeneration through a cell/GF-free, one-step surgery, and thus, these scaffolds demonstrate high potential for clinical translation in the treatment of massive bone defects, while circumventing the issues associated with stem cell transplantation and autografting. More importantly, the present study provides a scientific basis and preliminary understanding of the biological mechanism underlying the effects of nSCs on in situ bone regeneration, which will provide insights and future research platforms for examining the effects of silicon ion- or other metallic ion-containing nanostructures in cell–material interactions.

Experimental Section

Experimental details can be found in the Supporting Information.

Supporting Information

Supporting Information is available from the Wiley Online Library or from the author.

Acknowledgements

S.-J.W., D.J., and Z.-Z.Z. contributed equally to this work. This work was supported by the National Natural Science Foundation of China (Nos. 51773004, 81630056, 51273004, and 31200725) and National Key Research and Development Program (No. 2016YFC1100704).

Conflict of Interest

The authors declare no conflict of interest.

Keywords

bone regeneration, collagen, mesenchymal stem cells, scaffolds, surface biosilicification

Received: July 8, 2019
Revised: September 26, 2019
Published online: October 17, 2019

[1] a) D. E. Discher, P. Janmey, Y. L. Wang, *Science* **2005**, *310*, 1139; b) A. J. Ridley, M. A. Schwartz, K. Burridge, R. A. Firtel, M. H. Ginsberg, G. Borisy, J. T. Parsons, A. R. Horwitz, *Science* **2003**, *302*, 1704; c) S. J. Hollister, *Nat. Mater.* **2005**, *4*, 518.

[2] a) B. A. Julian, D. A. Laskow, J. Dubovsky, E. V. Dubovsky, J. J. Curtis, L. D. Quarles, *N. Engl. J. Med.* **1991**, *325*, 544; b) W. F. Enneking, E. R. Mindell, *J. Bone Jt. Surg.* **1991**, *73*, 1123; c) M. Marcacci, E. Kon, V. Moukhachev, A. Lavroukov, S. Kutepov, R. Quarto, M. Mastrogiacomo, R. Cancedda, *Tissue Eng.* **2007**, *13*, 947.

[3] a) K. I. Lee, J. S. Lee, K. T. Kang, Y. B. Shim, Y. S. Kim, J. W. Jang, S. H. Moon, D. D. D'Lima, *Am. J. Sports Med.* **2018**, *46*, 1641; b) D. Seow, Y. Yasui, E. T. Hurley, A. W. Ross, C. D. Murawski, Y. Shimozono, J. G. Kennedy, *Am. J. Sports Med.* **2018**, *46*, 1758; c) F. Sharmin, C. McDermott, J. Lieberman, A. Sanjay, Y. Khan, *J. Orthop. Res.* **2017**, *35*, 1086; d) W. F. Willems, M. Larsen, G. Giusti, P. F. Friedrich, A. T. Bishop, *J. Orthop. Res.* **2011**, *29*, 1431; e) M. D. Hoffman, C. Xie, X. P. Zhang, D. S. W. Benoit, *Biomaterials* **2013**, *34*, 8887.

[4] a) G. Tommasi, S. Perni, P. Prokopovich, *Tissue Eng., Part A* **2016**, *22*, 862; b) H. Takeuchi, Y. Niki, H. Matsunari, K. Umeyama, H. Nagashima, H. Enomoto, Y. Toyama, M. Matsumoto, M. Nakamura, *Am. J. Sports Med.* **2016**, *44*, 2375; c) Z. Wang, Y. Wang, Z. Y. Wang, J. S. Gutkind, Z. L. Wang, F. Wang, J. Lu, G. Niu, G. J. Teng, X. Y. Chen, *Stem Cells* **2015**, *33*, 456.

[5] a) C. E. Goldring, P. A. Duffy, N. Benvenisty, P. W. Andrews, U. Ben-David, R. Eakins, N. French, N. A. Hanley, L. Kelly, N. R. Kitteringham, *Cell Stem Cell* **2011**, *9*, 176; b) W. L. Grayson, B. A. Bunnell, E. Martin, T. Frazier, B. P. Hung, J. M. Gimble, *Nat. Rev. Endocrinol.* **2015**, *11*, 140.

[6] a) Y. R. Yun, J. H. Jang, E. Jeon, W. Kang, S. Lee, J. E. Won, H. W. Kim, I. Wall, *Regener. Med.* **2012**, *7*, 369; b) E. J. Carragee, E. L. Hurwitz, B. K. Weiner, *Spine J.* **2011**, *11*, 471; c) Q. Q. Han, Y. Du, P. S. Yang, *Future Med. Chem.* **2013**, *5*, 1671; d) C. L. Chaffer, N. D. Marjanovic, T. Lee, G. Bell, C. G. Kleer, F. Reinhardt, A. C. D'Alessio, R. A. Young, R. A. Weinberg, *Cell* **2013**, *154*, 61.

[7] a) S. W. Lane, D. A. Williams, F. M. Watt, *Nat. Biotechnol.* **2014**, *32*, 795; b) S. Pina, J. M. Oliveira, R. L. Reis, *Adv. Mater.* **2015**, *27*, 1143; c) R. J. McMurray, N. Gadegaard, P. M. Tsimbouri, K. V. Burgess, L. E. McNamara, R. Tare, K. Murawski, E. Kingham, R. O. C. Oreffo, M. J. Dalby, *Nat. Mater.* **2011**, *10*, 637; d) J. R. Xavier, T. Thakur, P. Desai, M. K. Jaiswal, N. Sears, E. Cosgriff-Hernandez, R. Kaunas, A. K. Gaharwar, *ACS Nano* **2015**, *9*, 3109; e) Y. Liu, S. A. Liu, D. Luo, Z. J. Xue, X. A. Yang, L. Cu, Y. H. Zhou, T. Wang, *Adv. Mater.* **2016**, *28*, 8740.

[8] a) X. Zhou, F. M. Moussa, S. Mankoci, P. Ustriyana, N. Zhang, S. Abdelmagid, J. Molenda, W. L. Murphy, F. F. Safadi, N. Sahai, *Acta Biomater.* **2016**, *39*, 192; b) V. G. Varanasi, T. Odatsu, T. Bishop, J. Chang, J. Owyoung, P. M. Loomer, *J. Biomed. Mater. Res., Part A* **2016**, *104*, 2604; c) A. Ilyas, T. Odatsu, A. Shah, F. Monte, H. K. Kim, P. Kramer, P. B. Aswath, V. G. Varanasi, *Adv. Healthcare Mater.* **2016**, *5*, 2199; d) 1. S. Heinemann, C. Heinemann, M. Jager, J. Neunzehn, H. P. Wiesmann, T. Hanke, *ACS Appl. Mater. Interfaces* **2011**, *3*, 4323; e) G. M. Cunniffe, G. R. Dickson, S. Partap, K. T. Stanton, F. J. O'Brien, *J. Mater. Sci.: Mater. Med.* **2010**, *21*, 2293.

[9] a) A. K. Gaharwar, S. M. Mihaila, A. Swami, A. Patel, S. Sant, R. L. Reis, A. P. Marques, M. E. Gomes, A. Khademhosseini, *Adv. Mater.* **2013**, *25*, 3329; b) J. L. Sun, K. Jiao, L. N. Niu, Y. Jiao, Q. Song, L. J. Shen, F. R. Tay, J. H. Chen, *Biomaterials* **2017**, *113*, 203; c) H. R. Luckarift, M. B. Dickerson, K. H. Sandhage, J. C. Spain, *Small* **2006**, *2*, 640; d) K. Jiao, L. N. Niu, Q. H. Li, F. M. Chen, W. Zhao, J. J. Li, J. H. Chen, C. W. Cutler, D. H. Pashley, F. R. Tay, *Acta Biomater.* **2015**, *19*, 23; e) S. D. Pogula, S. V. Patwardhan, C. C. Perry, J. W. Gillespie, S. Yarlagadda Jr., K. L. Kiick, *Langmuir* **2007**, *23*, 6677; f) D. J. Kim, K. B. Lee, Y. S. Chi, W. J. Kim, H. J. Paik, I. S. Choi, *Langmuir* **2004**, *20*, 7904.

[10] a) Z. Zhang, M. J. Gupte, P. X. Ma, *Expert Opin. Biol. Ther.* **2013**, *13*, 527; b) E. L. Fong, B. M. Watson, F. K. Kasper, A. G. Mikos, *Adv. Mater.* **2012**, *24*, 4995; c) E. Alarcin, X. F. Guan, S. S. Kashaf, K. Elbaradie, H. Z. Yang, H. L. Jang, A. Khademhosseini, *Regener. Med.* **2016**, *11*, 849; d) G. I. Im, *Tissue Eng., Part B* **2016**, *22*, 160.

[11] e) W. Chen, S. He, W. Pan, Y. Jin, W. Zhang, X. Jiang, *Chem. Mater.* **2010**, *22*, 6212; f) V. Karageorgiou, D. Kaplan, *Biomaterials* **2005**, *26*, 5474.

[12] S. Bose, S. Vahabzadeh, A. Bandyopadhyay, *Mater. Today* **2013**, *16*, 496.

[13] T. Coradin, O. Durupthy, J. Livage, *Langmuir* **2002**, *18*, 2331.

[14] M. Vallet-Regi, E. Ruiz-Hernandez, *Adv. Mater.* **2011**, *23*, 5177.

[15] M. J. Dalby, N. Gadegaard, R. O. Oreffo, *Nat. Mater.* **2014**, *13*, 558.

[16] S. F. Yan, J. B. Yin, L. Cui, Y. Yang, X. S. Chen, *Colloids Surf., B* **2011**, *86*, 218.

[17] R. Jugdaohsingh, A. I. Watson, L. D. Pedro, J. J. Powell, *Bone* **2015**, *75*, 40.

[18] K. D. Hankenson, K. Gagne, M. Shaughnessy, *Adv. Drug Delivery Rev.* **2015**, *94*, 3.

[19] a) P. J. Marie, E. Hay, Z. Saidak, *Trends Endocrinol. Metab.* **2014**, *25*, 567; b) P. J. Marie, *Nat. Rev. Endocrinol.* **2013**, *9*, 288; c) D. Zhu, Y. Su, M. L. Young, J. Ma, Y. Zheng, L. Tang, *ACS Appl. Mater. Interfaces* **2017**, *9*, 27453.

[20] a) A. Hayrapetyan, J. A. Jansen, J. J. van den Beucken, *Tissue Eng., Part B* **2015**, *21*, 75; b) R. Baron, M. Kneissel, *Nat. Med.* **2013**, *19*, 179; c) S. Midha, S. Murab, S. Ghosh, *Biomaterials* **2016**, *97*, 133; d) A. Spangenberg, N. Maghsoodi, D. Dulnoan, A. E. Moore, S. Edwards, M. L. Frost, G. Hampson, *Calcif. Tissue Int.* **2016**, *99*, 608.